**ISTITUTO NAZIONALE DI FISICA NUCLEARE**

**Sezione di Genova**

**INFN/TC-99/17**
**8 Ottobre 1999**

# THE DESIGN OF A GAS CERENKOV PARTICLE DETECTOR FOR THE GRAAL HIGH ENERGY POLARISED PHOTON FACILITY

M. Castoldi[1], R. Cereseto[1], A. Fantini[2], S. Farinon[1], M. Marchelli[1], D. Moricciani[3], G. Nobili[3], M. Olcese[1], M. Parodi[1], R. Puppo[1], C. Schaerf[3,4], A. Zucchiatti[1]

[1)]*INFN, Sezione di Genova – Via Dodecaneso 33, I–16146 Genova (Italy)*
[2)]*Dipartimento di Fisica, Università di Ferrara*
[3)]*INFN, Sezione Roma II*
[4)]*Dipartimento di Fisica, Università di Roma "Tor Vergata"*

**Abstract**

We discuss the design of a multi–mirror gas Cerenkov counter to be added to the existing GRAAL apparatus at the European Synchrotron Radiation Facility in Grenoble. The guidelines of the project are reviewed and their impact on the mechanical design is outlined. Several technical procedures adopted to design the bank of mirrors and their support: computer aided engineering (CAE), optical ray–tracing, materials selection, are discussed in detail. Structural analysis has been done to assess reproducibility of optical performances of the detector.

PACS.: 29.40.K, 42.15.E, 46.70.D

*Published by* ***SIS–Pubblicazioni***
*Laboratori Nazionali di Frascati*

## 1. INTRODUCTION

The GRAAL beam (GRenoble Anneau Accelerateur Laser) is a high energy (1.6 GeV maximum) photon beam [1),2)] obtained through the back scattering of laser photons by the 6 GeV electrons circulating in the storage ring of the ESRF (European Synchrotron Radiation Facility) in Grenoble.

The experimental set-up, named LAGRANGE [3),4),5)], associated to the GRAAL beam covers a solid angle very close to $4\pi$ steradians by a system of several detectors deployed in three contiguous regions:

1. a forward one lying between 2 and 25 degrees with respect to the beam axis and consisting of plane wire chambers, a wall of plastic scintillators and a sampling electromagnetic calorimeter
2. a central detector covering angles between 25 and 155 degrees consisting of cylindrical wire chambers, scintillator bars and a BGO calorimeter
3. a backward one covering angles between 155 and 178 degrees consisting of plastic scintillator discs

A sketch of existing detectors is given in figure 1.

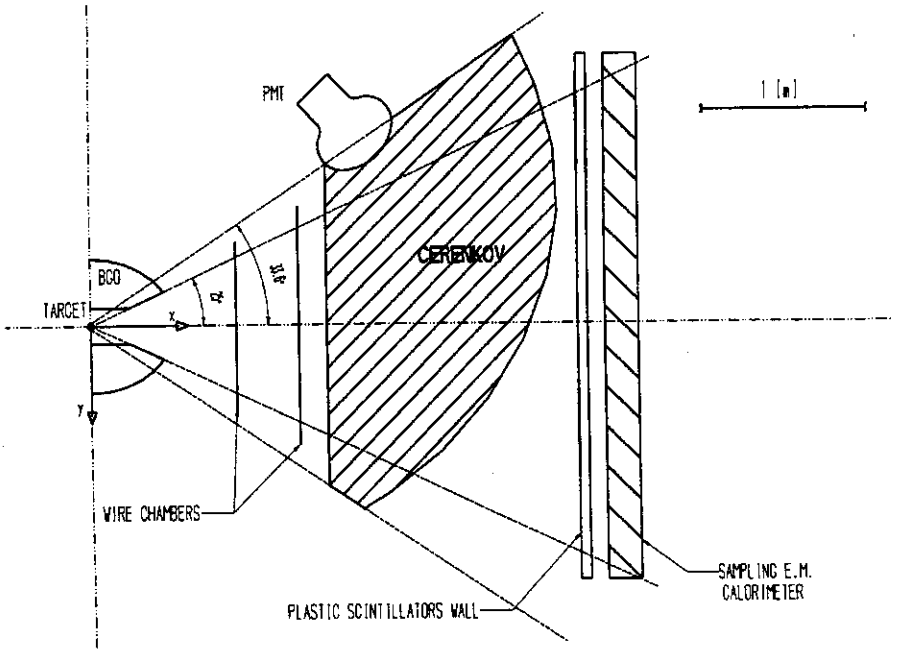


**FIGURE 1:** A plan view of the LAGRANGE apparatus showing the largest existing detectors in the forward and central region. The beam direction is coincident with the x-axis. Also shown are the ideal reflecting ellipsoid and the approximate space (dashed area) occupied by the Cerenkov detector.

The apparatus is well suited to the study of nuclear reactions, because of its high efficiency to charged and neutral particles, the almost complete coverage (99%) of the solid angle and the redundant information on particle trajectories, type and energy. However there was justification for upgrading the actual detector assembly for the forthcoming experimental program. This was done in order to assure identification of events in which electrons and positrons are produced by the photon beam interacting in the target or with materials along the beam line. This background is emitted essentially in the forward direction and can have significant effects in some of our measurements.

Cerenkov counters are commonly used for the identification of electrons. Being based on the collection of low intensity light it will require, in our case, a large detector both optically tuned and mechanically stable. We report here on the design of such detector, which is now being produced at INFN, where CAE (Computer Aided Engineering) technology, optical ray-tracing and structural analysis have been extensively used. Consideration has been given to selection of materials with regards to their effects on particles background.

## 2. GUIDELINES OF THE DETECTOR DESIGN

### 2.1 Detector type and features

The working principle of a Cerenkov detector is well known. In a medium of refraction index $n$ a charged particle with velocity $v=\beta c>c/n$ ($c$ being the velocity of light in vacuum) will emit an electromagnetic plane wave (mostly ultraviolet photons) at an angle $\theta_c=\arccos(1/\beta n)$ with respect to the particle direction. If the particle velocity is $v<\beta=1/n$ there is no light emission. In the so-called threshold Cerenkov counter, by using an appropriate medium, one can set a threshold velocity $\beta_t$ that will not be reached by heavy particles such as muons, pions and protons, while electrons will be above threshold even at low momentum and will therefore produce a signal usable as a veto in the event trigger. We have decided to adopt this kind of detector for our experiment upgrade. The guidelines for this detector were:

1. A medium with a refraction index suitable for discrimination between electrons and heavier charged particles, in the GRAAL energy range. The medium should be chemically inert, non toxic and non flammable and present a small interaction probability for the crossing particles.
2. Dimensions compatible with placement in the forward section of LAGRANGE, ahead of the plane wire chambers and before the plastic scintillator wall, but also having a sufficiently long particle path to generate enough Cerenkov photons for high detection efficiency.
3. A support structure, rigid enough to keep unaltered the optical performance of the detector during installation and use, but also sufficiently light-weight to avoid unnecessary inactive material along the particle path that could result, especially for the heavier particles, in significant energy losses.
4. An optical system able to focus on the cathode of a convenient photomultiplier (PMT), the Cerenkov light produced by particles with directions between 0 and 25 degrees, but again light-weight to avoid unnecessary inactive material.

### 2.2 Choice of the radiator

A gas is the most suitable medium. The refractive index is close to 1 and hence there is a high $\beta_t$ threshold. It also has a low density, resulting in negligible energy losses for charged hadrons. We have chosen the tetra-fluoro-butane $C_4F_{10}$ which has a refraction index $n$ = 1.0015, at atmospheric pressure, corresponding to a threshold velocity $\beta_t$ = 0.9985. Given the electron, muon and pion masses $m_e$ = 0.511 MeV, $m_\mu$ = 105.66 MeV, $m_\pi$ = 139.57 MeV, the energies at which the three particles have a velocity greater than $\beta_t$ are respectively:

$$E_e = \frac{m_e c^2}{\sqrt{1-\beta_t^2}} = 9.33\,\text{MeV};\ E_\mu = \frac{m_e c^2}{\sqrt{1-\beta_t^2}} = 1929\,\text{MeV};\ E_\pi = \frac{m_\pi c^2}{\sqrt{1-\beta_t^2}} = 2549\,\text{MeV} \qquad (1)$$

At energies made possible by the GRAAL beam, for electrons and pions within the event trigger, we will always have $\beta_\pi < \beta_\mu < \beta_t < \beta_e$. The angle, with respect to the electron trajectory, at which the Cerenkov light will be emitted in $C_4F_{10}$ is:

$$\vartheta_M = \text{acos}\left(\frac{1}{n}\right) = 3.17^\circ \qquad (2)$$

The number of photons emitted per unit path length and unit wavelength along the trajectory is given by:

$$\frac{dN}{dx d\lambda} = 2\pi\alpha \frac{1}{\lambda^2}\left(1 - \frac{1}{\beta^2 n^2}\right) \qquad (3)$$

where $\alpha$ is the fine structure constant. The energy spectrum of the emitted light is peaked towards the short wavelengths and $C_4F_{10}$ is conveniently transparent to UV light

## 3. THE CERENKOV DESIGN

### 3.1 Basic design choices

To produce the mechanical and optical design, Computer Aided Engineering packages have been extensively used. The existing set-up, has been described in a co-ordinate system originating from the target centre, having the $x$-axis along the beam path, the $y$-axis pointing towards the centre of the ESRF synchrotron and the $z$-axis pointing to the floor. Some constraints determine the general detector layout seen in figure 1. Cerenkov photons can be emitted along any particle trajectory within the cone that has its axis coincident with the beam direction and an aperture of 25 degrees. They should be focused, by reflection, onto one photomultiplier (PMT) because there is no room in the experimental area to locate more. The PMT must be as far as possible from the reflector to improve the focusing of photons emitted by particles travelling around the extreme trajectories and outside the forward 25 degrees cone to avoid the production of light by pions in the PMT window. It must have a large size to compensate for the spread introduced by emission of light at 3.17° from the electron trajectory and to allow tolerances on the radius of curvature and discontinuities of the reflecting surface. We have

chosen the Hamamatsu R3600-06 PMT with a boron-silicate window and a spherical photo-cathode providing a sensitive circular cross section of 460 mm diameter. The simplest reflection surface compatible with the given constraints is a rotation ellipsoid. This will have the major axis tilted with respect to the beam axis and the two foci will correspond to the target and the photo-cathode centres. It will finally be tangent to a plane parallel to the plastic scintillators wall, to make room for the support frame. Due to tilting, the region filled with the $C_4F_{10}$ gas will not be symmetric with respect to the beam axis (dashed area of figure 1). As the number of emitted Cerenkov photons depends on the path length and therefore on the emission direction, it is desirable to reduce path differences. This can only be achieved if the tilting angle is minimum and if the PMT is as close as possible to the target. The best option is tilting the ellipsoid axis by -33.6 degrees, placing the PMT cathode centre at (1650 mm, -1100 mm, 0 mm) and imposing a minimum clearance of 30 mm from the end of the Cerenkov to the plastic scintillator wall.

The complexity of the construction of a rotation ellipsoid, of large dimensions and adequate reflectivity, has suggested a modular solution, with several mirrors. The design has been oriented to the highest possible degree of standardisation, to a simple mirror shape and to a mechanical support structure easy to fabricate and to optically align. The use of light materials and structures has been taken as the design major driving issue. A bank of uniform thickness, large radius, spherical Plexiglas® mirrors with square section, coated with aluminium and supported by a light tubular global frame has been chosen.

### 3.2 The mirrors

With the aid of the Pro-Engineer package by Parametric Technology Corporation [6] we have produced a 3D model of the existing experimental set-up in order to define the space available for placement of the Cerenkov. The mirrors bank has been designed by approximating the ideal reflective surface with spherical bowl mirrors having a square section. The mirror size has been chosen so to minimise the number of mirrors (106) and to make them compatible with the tooling used for the coating process. The pattern (figures 2 and 5) is determined by aligning the central mirror on its ideal position and then producing edge overlap of the other mirrors in the central column by keeping their centres on a vertical plane and shifting the mirrors alternatively back and forth. The same has been done for the other columns, proceeding from the centre to the sides and assuring overlap by shifting the columns alternatively back and forth.

Two different configurations have been investigated as regards the geometrical loss of coverage, the mirrors overlap and the particle energy loss. They correspond to a shorter and larger distance between the columns (configuration N or *W* respectively). The two sets are given in Table 1. The loss of coverage of the reflective surface and the percent overlap are given as well in Table 1. The largest losses of geometrical coverage are experienced at the extremes of the mirror bank (close to 25 degrees) while the average value is rather good in both configurations. A 1.4% average overlap must be added due to rows overlap.

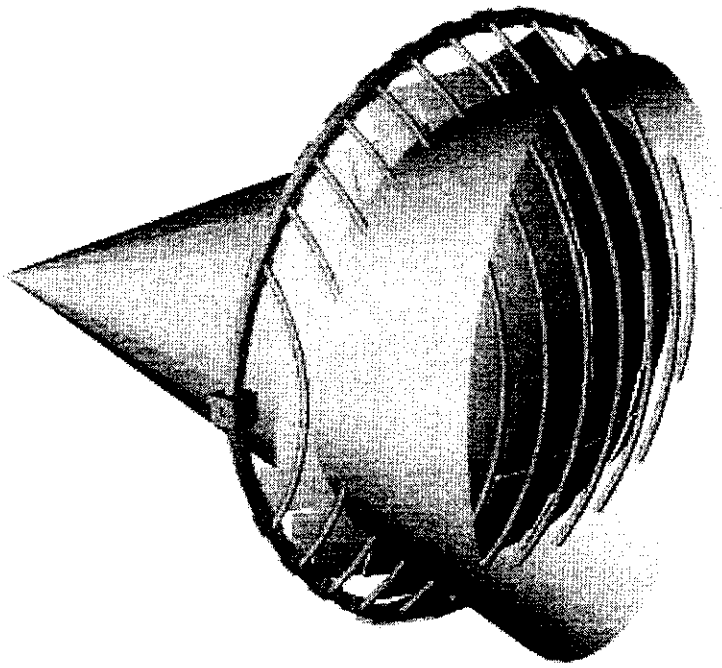

**FIGURE 2**: The mirror bank (light grey), as positioned in the CAE with the interception of the 25 degrees particles emission cone. The vertical span of the bank is 2.82 m. Also shown (dark grey) is the global support frame consisting of vertical ribs and of the external tubular structure.

**TABLE 1:** The approximation of the ellipsoid for two choices of the distance between columns of mirrors.

| Set | Average Loss of Coverage | Max Loss of Coverage | Average Overlap | Max Overlap | Distances between columns [mm] |
|---|---|---|---|---|---|
| *N* | *0.2%* | *1.5%* | *2.3% + 1.4%* | *7.3%* | *238-237-247-245-235-235-202-211-169-182-137* |
| *W* | *0.7%* | *6.9%* | *1.2% + 1.4%* | *2.7%* | *238-237-247-245-236-238-211-216-176-186-138* |

Each mirror is manufactured through a three phase process. A Plexiglas® sheet, 3mm thick, is shaped as a spherical bowl by thermal formation in a male-female mould and cut to a rectangular projection of $252 \pm 0.2$ mm by $262.6 \pm 0.2$ mm. The raw sheet is then coated on the concave surface with a 100 nm aluminium layer followed by a 100 nm protective coating (Alflex®-UV Special by Balzers GmbH). The coating process requires heating of the pre-formed Plexiglas® to about 50 °C for approximately an hour. The manufacturer guarantees a reflectivity larger than 80% at a wavelength of 300nm, in not less than 90% of the treated pieces. The final steps will consist in making the mirror projection a square of $252 \pm 0.2$ mm ( by cutting the excess material needed to hold the pieces for coating ) and then gluing the local support at the back, at room temperature and with an epoxy resin.

CMM (Co-ordinate Measuring Machine) measurements have been made on a limited series of prototypes to determine the radius of curvature and the deviation of the reflection surface from the nominal one (shape tolerance) in order to fix the tolerance limits and to quantify the distortions introduced by the thermal cycle of the aluminium coating process. We have seen that starting from a radius of $2700 \pm 100$ mm (after thermal formation) we reach, after surface coating, a radius of $1900 \pm 100$ mm, which fulfils the condition of good focusing of Cerenkov light. The shape deviations from the nominal surface have been found negligible: maximum sphericity error between 0.15mm and 0.26mm.

### 3.3 The global frame

The vertical planes, that contain mirror centres, are made parallel to the GRAAL beam axis, and their intersections with the ideal ellipsoid, in the region occupied by the mirrors, are well approximated by circumference arcs. These geometrical properties allow to design a support frame made of light aluminium tubes (1 mm wall thickness), shaped as circumference arcs of a different radius, parallel to one another and sitting on vertical planes. The mirrors global frame is shown in figure 2 and 4. It consists of 12 tubular arcs (ribs), parallel to one another, flanged on three tubular arcs with square section, sitting on a vertical plane and completely out of the 25 degrees cone. The square section tubular arcs are interrupted and connected to a flat slab at the bottom of the detector due to space limitations.

### 3.4 Connecting mirrors to the global frame.

The use of round section vertical ribs, facilitates the mirrors alignment. The mirror local support (figure 3) has been designed to provide easy adjustments of the mirrors positions and orientations. It allows:

(1) vertical displacement of the mirror centre,
(2) rotation of the mirror surface with respect to a vertical axis,
(3) displacement of the mirrors surface along the normal to the ideal reflecting surface in that point,
(4) mirror orientation through a spherical joint.

The alignment procedure will consist of two subsequent steps:

- each mirror will be positioned relative to the rest of the bank (steps 1, 2, 3 above), to warrant the coverage of the entire surface
- final precise adjustment of each mirror (step 4), acting on the spherical joint

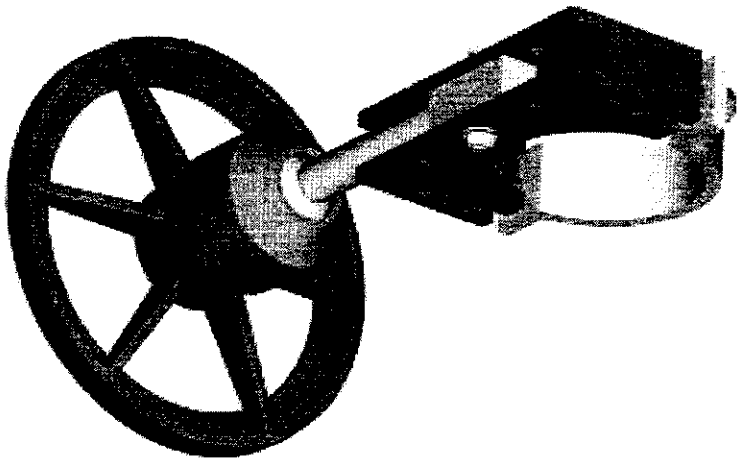

**FIGURE 3:** A view of the mirror local support. Light grey parts are aluminium, dark grey parts are composite material made of Nylon (PA 66) reinforced with 40% of carbon fibres while the joint is aluminium. The composite disk has a diameter of 80 mm.

### 3.5 The detector basement

The three square section arcs constitute the external frame of the mirrors bank. They will be connected to the basement of the detector, through two pivots sitting on the horizontal symmetry plane. The basement will also assure the positioning and holding of the PMT. The base frame (shown in figure 4) is coupled through ball-bush bearings to two round-section straight guides, bolted to the experimental room floor. The two pivots, that connect the global frame and the base, allow a rotation of the entire mirror bank around the symmetry axis identified by the pivots. The straight rails, will allow displacement of the entire Cerenkov detector with respect to the GRAAL beam, while the tubular frame could be uncoupled from the base, by removing the two pivots for complete clearance of the 25 degrees cone and free access to other detectors.

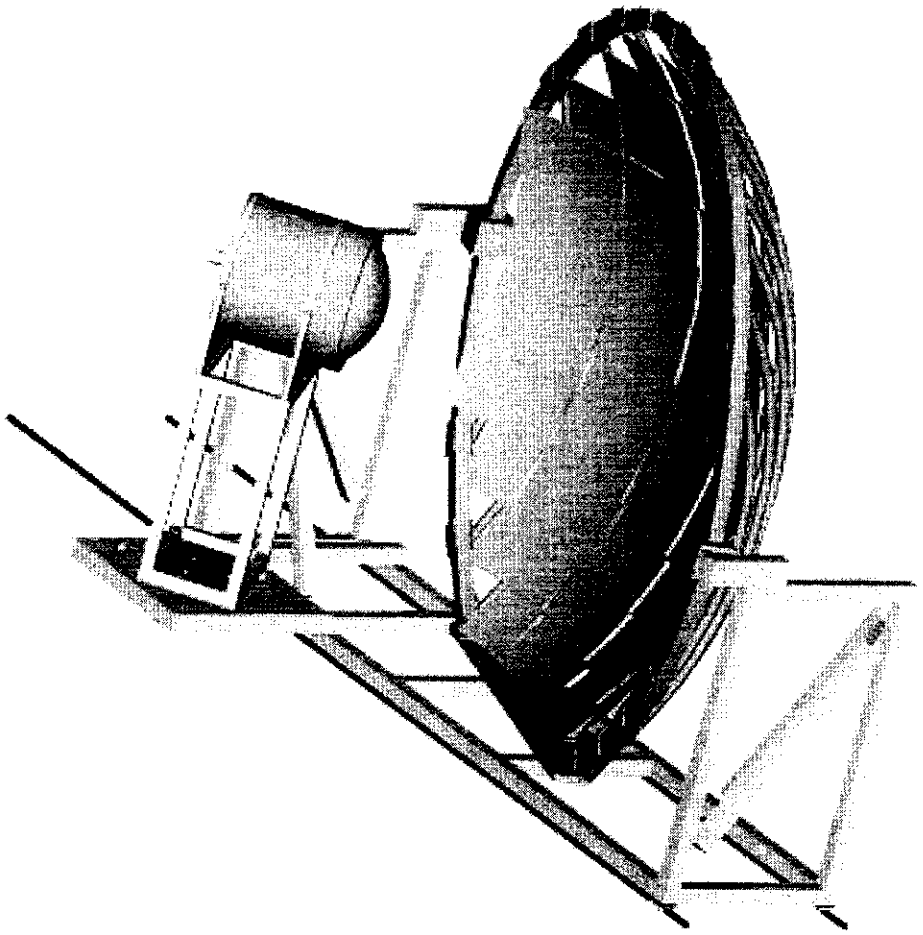

**FIGURE 4:** The aluminium detector basement (light grey) on the straight rails provided for detector movement. Also shown are the global support frame (dark grey), the mirror bank and, on the left, the PMT housing. The horizontal span of the basement is 3.23 meters.

## 4. OPTICAL PERFORMANCE OF THE MIRROR BANK

### 4.1 Collection of photons

The optical performance of the mirror bank has been checked with the code Optica [7] that performs ray-tracing (figure 5) in complex optical systems. We have studied the light collection for 5 values of the mirror radius of curvature in configuration *N* and two cases for configuration *W*. We have randomly extracted 60 particle trajectories for each case, within the 25 degrees cone. Inside the Cerenkov volume we have forced the emission, along the trajectory, of cones of rays (of 3.17 degrees aperture) in numbers proportional to

the path length. No wavelength selection has been performed and for all photons a 100% mirror reflectivity has been assumed. The results of the ray tracing are given in Table 2, where the fraction of generated rays reflected by the mirrors and the fraction of reflected rays lost by the PMT are given. A few more particle trajectories, directed specifically towards areas non completely covered by superposed mirrors, have also been followed. For these trajectories we have calculated light losses close to 20-25%.

**TABLE 2:** Results of the optical ray-tracing.

| Curvature Radius | Columns Spacing | Mirrors reflection [%] Min. - Average - Max. | | | PMT loss [%] Min. -Average - Max. | | |
|---|---|---|---|---|---|---|---|
| *1100 mm* | *N* | *95.3* | *99.0* | *100* | *0.0* | *6.6* | *20.9* |
| *1500 mm* | *"* | *97.4* | *98.8* | *100* | *0.0* | *0.2* | *1.3* |
| *1900 mm* | *"* | *91.7* | *97.6* | *100* | | *0* | |
| *2700 mm* | *"* | *95.6* | *98.4* | *100* | | *0* | |
| *3500 mm* | *"* | *92.3* | *97.1* | *99.5* | *0.0* | *0.3* | *2.0* |
| *1900 mm* | *W* | *96.0* | *98.5* | *100* | | *0* | |
| *2700 mm* | *"* | *92.7* | *97.8* | *100* | | *0* | |

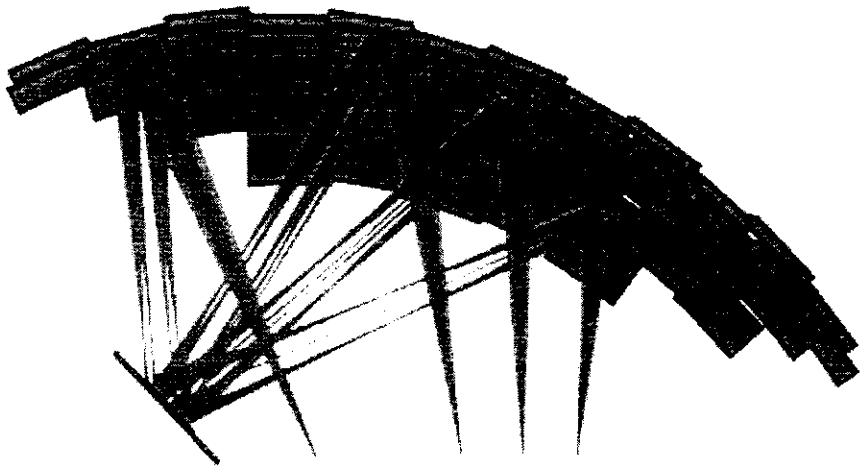

**FIGURE 5:** An example of ray tracing performed by the Optica package showing the good collection of rays by the photo-cathode. The mirror curvature radius is 1900 mm.

Two conclusions can be drawn from table 2:

1. Almost 98% of the photons impinge on the mirror bank; slightly more for configuration *N*. They will be reflected according to their wavelength.
2. The collection of reflected photons by the PMT is complete for radii of curvature between 1900 and 2700 mm, while losses up to 21% are experienced at 1100 mm, and the coverage of the PMT is at the limit for 1500 mm and 3500 mm.

The configuration with shorter distance between the columns is preferable, even because a larger superposition of mirrors does not affect too much the particle energy spectra, as we will see later. Eventually, an even better coverage of the ideal reflecting surface could be achieved, at the time of final mirror alignment using all the degrees of freedom allowed by the local mirror support.

### 4.2 Conversion of photons

We can finally estimate the number of photo-electrons produced at the PMT cathode. The integration of equation (3) gives:

$$N = \iint 2\pi\alpha \frac{1}{\lambda^2}\left(1 - \frac{1}{\beta^2 n^2}\right) R(\lambda)T(\lambda)Q(\lambda)K_M K_P dx d\lambda \qquad (4)$$

where $R(\lambda)$ is the reflectance of the mirror coating, $T(\lambda)$ is the transmission of the boron-silicate PMT window, $Q(\lambda)$ is the cathode quantum efficiency. $K_M$ is the average geometric collection of photons by the mirror bank and $K_P$ the average geometric collection of photons by the photo-cathode. With a radius of curvature between 1900 and 2700 mm $K_M > 97.6\%$ and $K_P = 100\%$. Taking into account the sensitivity curve (type 400K) given by Hamamatsu for the R-3600-06 PMT, the reflectivity of aluminium coated with Alflex®-UV Special and the minimum and maximum path possible in $C_4F_{10}$, we calculate a number of photoelectrons between 47 and: adequate for detection of electron background.

## 5. PARTICLE ENERGY LOSSES

The use of light materials is imposed by the need of avoiding energy degradation of heavy particles crossing the Cerenkov counter. Plastic materials have been used extensively, in the mirrors, their support, the $C_4F_{10}$ sealed chamber. In Table 3 we give, a summary of the main components of the Cerenkov detector and their extent in the 25 degrees active area. We have computed to first order the discrete energy losses for protons of different kinetic energies from 10 to 200 MeV. We have ignored the angular dependence of the energy losses and the non isotropic distribution of materials. The contribution of the thin plastic foil (Tedlar®) entry and exit windows (37.5 μm each) and the $C_4F_{10}$ gas is negligible. Pions of the same energy suffer lower specific energy losses. For mono-energetic incoming protons of 20, 40, 80, 150, 300 and 500MeV we computed the discrete energy spectrum after crossing the detector, as seen in figure 6. At 20 MeV the protons are either absorbed or loose more than half of their energy. From 40 MeV two main structures are seen in the spectra: the peak close to the incoming energy value is due to energy loss through a single layer of coated mirror; the other peak is due to energy loss through mirrors and ribs and would approach the first if more expensive carbon fibre ribs were used (red curves).

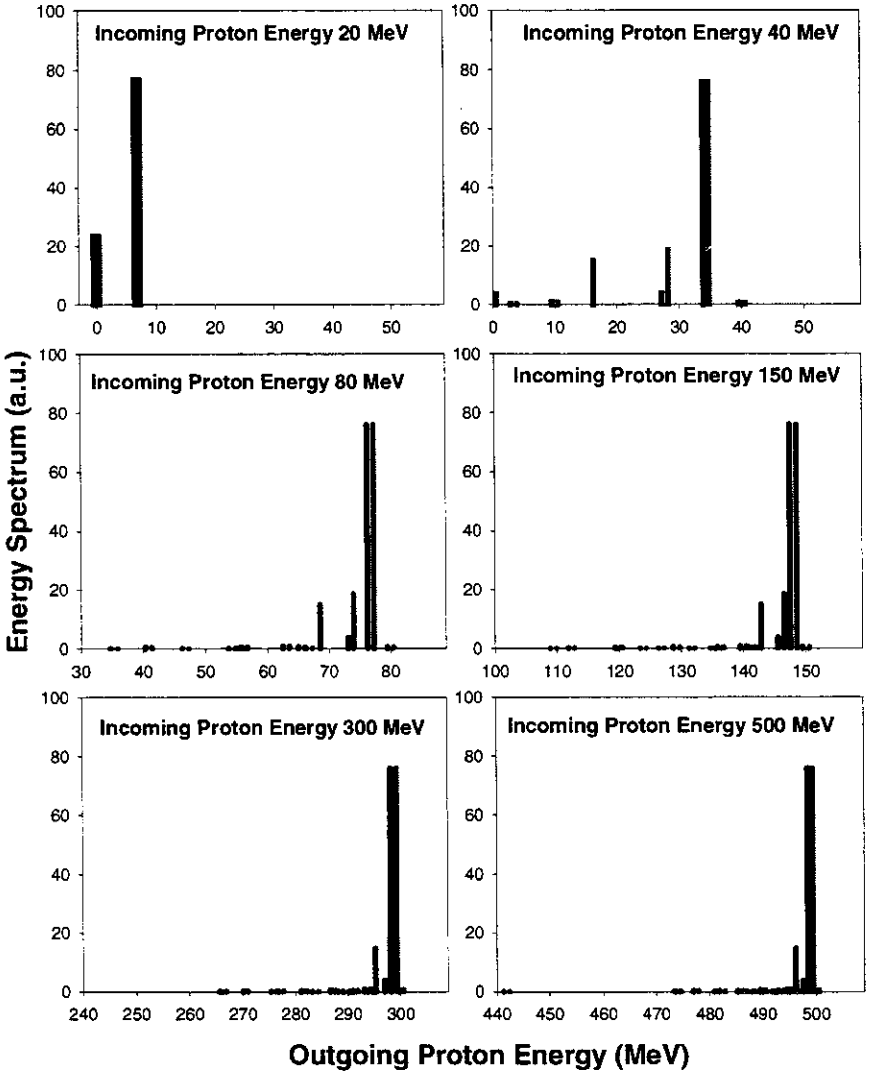


**FIGURE 6:** The energy spectra of mono–energetic protons passing through the Cerenkov materials for a few values of the incoming proton kinetic energy. In black with aluminium ribs, in grey with carbon fibre ribs.

The ratio between the two peaks changes only slightly between configuration *N* and configuration *W*. Although this double peak structure is observed at all energies we can say that distortion of proton spectra begins to be negligible above 80-100 MeV. For pions the losses will be lower. This situation in satisfactory for the range of experiments planned at GRAAL. As regards electrons, the use of low Z materials makes the absorbing media quite thin in terms of radiation lengths; therefore less than 1% of the incident electrons will radiate before reaching the plastic scintillator wall.

**TABLE 3:** Inactive materials crossed by particles in the 25 degrees cone. Two configurations of the mirror bank (N and W) were considered.

| **Type of piece** | **Material** | **Percent of surface in ± 25° cone** |
|---|---|---|
| *Coated mirror only* | Plexiglas® + 100 nm aluminium coating | *76.11 (W)*<br>*74.98 (N)* |
| *Local mirror support overlapping coated mirror and vertical rib* | Nylon (PA 66) reinforced with 40% carbon fibres + aluminium shaft + aluminium collar + steel bolts +portion of aluminium rib +portion of coated mirror | *6.02* |
| *Vertical rib overlapping coated mirror* | Aluminium + Plexiglas® + 100 nm aluminium coating | *14.85* |
| *Two coated mirrors overlapping* | Plexiglas® + 100 nm aluminium coating ( twice) | *2.56 (W)*<br>*3.69 (N)* |
| **Total surface in 25 degrees cone 44528 cm²** | | *100* |

## 6. STRUCTURAL ANALYSIS

In order to understand the misalignments of the mirror bank due to its own weight a structural finite element analysis has been performed using ANSYS code [8]. We have planned to align each mirror in sequence to simplify the mirror bank assembling. The procedure is correct as far as the initial alignment of the first mirror is not affected by the deflection of the support structure due to the weight of the whole mirror bank. The misalignment of each mirror is produced by two effects; the absolute displacement of the mirror centre and the rotation of the mirror axis relative to its nominal position. The purpose of the structural analysis has been to evaluate both contributions. The peculiar design of the global frame leads to a natural simplification of the FE (Finite Elements) model, which has been built using only beam elements. Due to light materials used for the mirror local supports, the centre of gravity of the mirror and local support ensemble is located very close to the geometric centre of the mirror. Therefore each mirror and its local support have been described with a no weight beam element having a length equal to the distance between the centre of gravity and the corresponding aluminium rib.

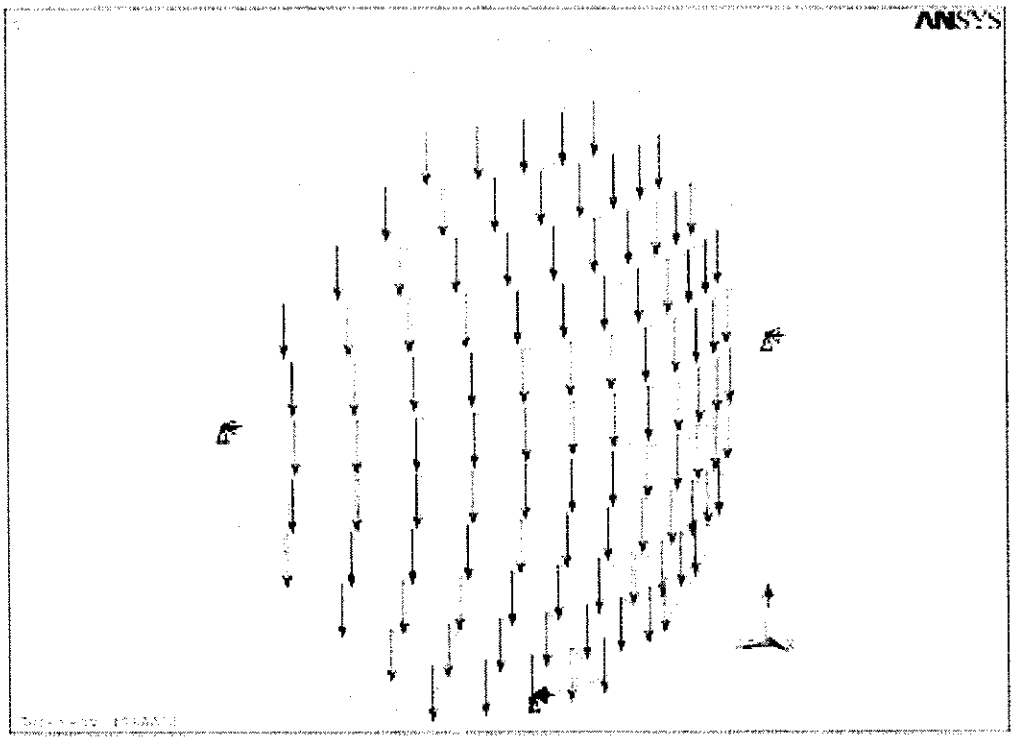


**FIGURE 7:** The support structure and the mirrors as schematically described in the structural analysis calculation.

The weight of the mirror and local support ensemble has been represented by an external force applied at the centre of gravity. All other concentrated loads, such as flanges and bolts have been distributed all along the tubular structure. We have assumed conservatively that the mirror bank and the global structure are supported in the vertical direction only at the two ends of the symmetry plane as shown in figure 7. Figure 8 shows the deformed shape of the global frame due to its weight: the maximum displacement of the mirror centre is 1.4 mm and occurs in the central position of the mirror bank. Figure 9 shows the rotation of each mirror relatively to its nominal position; the maximum value ($0.15^0$) corresponds to the mirror located at the top of the bank. Both the calculated displacements and the rotations are low enough to give a negligible effect on the mirror alignment.

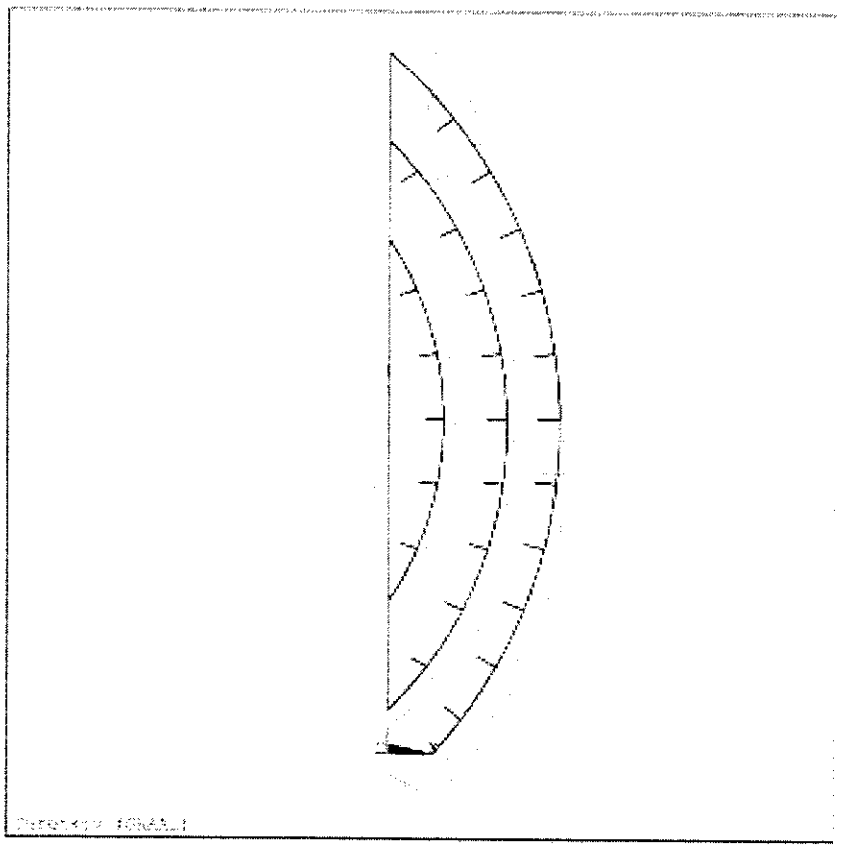

**FIGURE 8**: The structure deformation amplified 150 times.

## 7. CONCLUSIONS

We have designed a large surface gas Cerenkov threshold detector for the GRAAL nuclear physics facility, making extensive use of CAE and simulation tools. The adoption of simple geometrical constraints has led to a modular design. The detector designed is rather easy to produce, machine and install within the existing GRAAL apparatus. All parts of the detector: the mirrors, the intermediate support frame for the mirrors, the individual light support to connect each mirror to the intermediate frame and the base of the detector, have been studied to assure rigidity, optimum optical performances while making widespread use of light materials and of mechanically simple production processes.

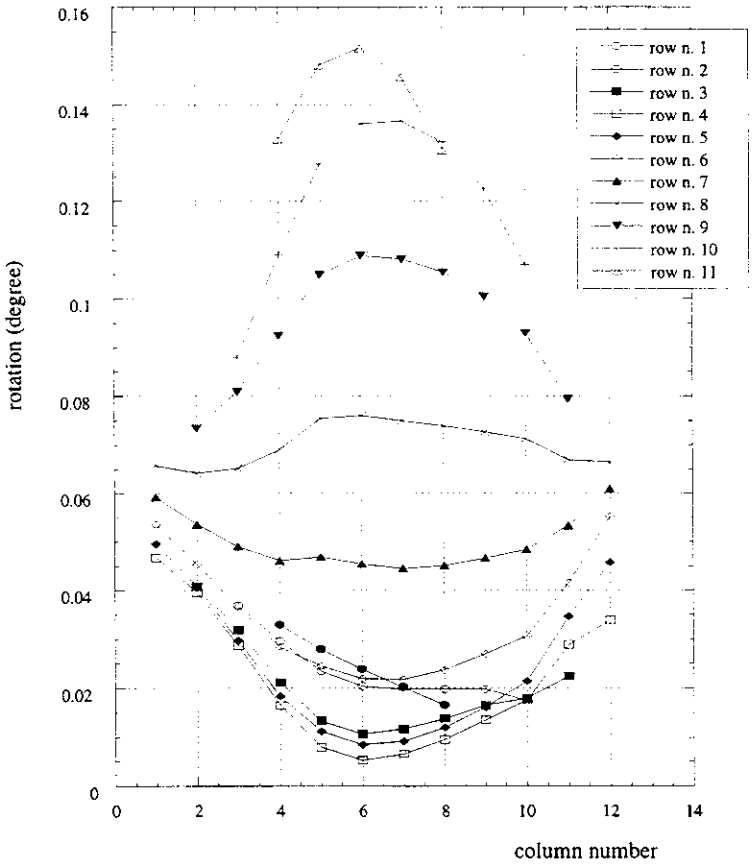


**FIGURE 9:** The rotation of mirrors due to the structure deformation. All mirrors are included and are divided by rows.

## 8. REFERENCES

(1) J.P. Bocquet et al., *Nucl. Phys. A622(1997)124c*
(2) J. Ajaka et al. *Proc. 12th Int. Symp on High Energy Spin Physiscs Amsterdam Sept 1996 World Scientific pg. 277*
(3) C. Schaerf, et al. *Proc. Int. Conf. on Perspectives in Hadr. Phys. - ICTP Trieste May 1997*
(4) M. Breueret al. *Proc. Ist ELFE Summer School- Cambridge 1995 Confinement Physics Editions Frontieres pg.319*
(5) F. Ghio et al., *Nucl. Instr. And Meth. A404(1998)71*
(6) Parametric Technology Corporation 128 Technology Drive Waltham MA 02154 USA
(7) Wolfram Research, Inc.100 Trade Center Drive Champaign, IL 61820-7237 USA
(8) Swanson Analysis System, Inc. P.O.Box 65 Johnson Rd Huston PA 15342-0065 USA